Climatology of Storm Reports Relative to Linear Jet Streaks

CHRISTOPHER J. SCHAFFER

Iowa State University, Ames, IA

Mentors: Dr. William A. Gallus Jr., Adam J. Clark

Iowa State University, Ames, IA

ABSTRACT

NCEP/NCAR NARR Reanalysis data, SPC storm reports, and an analysis of upper-level linear jet streaks by Johnson-O'Mara were used to examine the placement of storm reports associated with linear jet streaks over a ten-year period. The study also explores how average circulations within the jet streaks compare to the linear jet streak theory. It was found that tornado and hail reports tended to occur most frequently in the exit region away from the jet center, while wind reports were concentrated far from the major axis in the right entrance region. A low pressure center in the left exit region was the reason for the extensive surface convergence, and fronts associated with the low appeared to be a major reason for the storm report distributions and circulations observed. Convection and the tropopause height also appear to influence the jet streak circulations.

1. Introduction

Linear upper-level jet streaks tend to influence atmospheric circulations in a predictable way, causing upward motion in the right entrance and left exit regions, and downward motion in the left entrance and right exit regions (Uccellini and Johnson 1979; Brill et al. 1985; Hakim and Uccellini 1992). This theory of jet dynamics is considered by forecasters when anticipating the likelihood of severe weather. The goal of this study is to examine the climatology of storm reports relative to linear upper-level jet streaks using ten years of data from 1994 to 2003. The study will also investigate the area in and around the jet streaks to see how other factors alter the circulations associated with jet streaks and the related storm reports.

2. Background information

Explanations and observations of the circulations found in upper-level jet streaks have been provided by many researchers (Sechrist and Whittaker 1979; Uccellini and Johnson 1979; Bluestein and Thomas 1984; Keyser and Johnson 1984; Hakim and Uccellini 1992; Moore and Vanknowe 1992). It is understood that as air enters the entrance region of a jet streak, it becomes subgeostrophic. In order to accelerate, the ageostrophic wind moves the air to a lower height. It follows, then, that air in the right entrance region moves into the left entrance region. After passing the center of the jet streak, the air enters the exit region of the jet and becomes supergeostrophic. In order to decelerate, the air must move to a higher height.

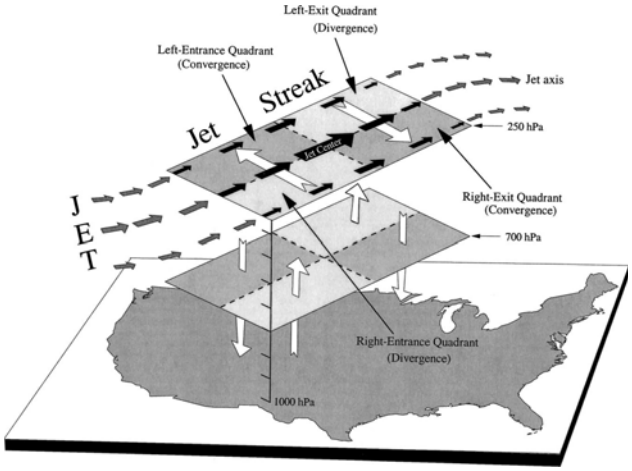

Fig. 1. An image from Rose el al. (2003) showing the circulations within and underneath an ideal linear jet streak. Permission granted by Dr. Mark Stoelinga, University of Washington, Seattle, WA.

This causes the air to move from the left exit region into the right exit region. These circulations are shown in Figure 1.

Uccellini and Johnson (1979), Brill et al. (1985), and Hakim and Uccellini (1992) have described the direct and indirect circulations that occur in the entrance and exit regions, respectively, of linear jet streaks (Fig. 1). Their studies have shown that as air converges in the left entrance and right exit regions, air is forced downward towards the surface. Likewise, as air diverges in the right entrance and left exit regions, air from lower altitudes moves upward into these regions. This upward motion may affect weather at the surface. Sechrist and Whittaker's (1979) case study showed that the largest divergence values aloft occurred at the same time that a surface cyclone was developing most rapidly.

Many authors have discussed the relationship between jet streaks aloft and severe weather at the surface. Keyser and Johnson (1984) observed that the intensification of two polar jet streaks appeared to contribute to severe weather from 0000 UTC 24 April 1975 to 1200 UTC 25 April 1975. Convective activity developed in the right exit region of the jet streak, then moved into the right entrance region. In the right entrance region, the convection developed into a MCC. They concluded that the diabatic heating within the MCC created a mesoscale circulation similar to that of the entrance region of the jet streak, enhancing the thermally direct circulation found in the entrance region. This diabatic heating may hide the true influence of jet streaks on dynamic circulations. Diabatic processes involving latent heat release can amplify the vertical motions associated with jet streak circulations (Uccellini and Kocin 1987). It is important to consider how diabatic processes affect the jet-induced motions.

While studying a particularly strong jet streak associated with tornados, large hail, and damaging winds, Bluestein and Thomas (1984) discovered that the storm responsible for the severe weather in this case formed under the exit region of the jet steak. At 1200 UTC (at least six hours before convection began), there was strong downward motion in the right exit region, and weak upward motion in the left exit region. By 0000 UTC, there was strong upward motion in the left exit region and strong downward motion in the right exit region. Furthermore, all areas of convection occurred within a kinematically-computed area of upward motion.

More recently, Rose et al. (2003) related tornado reports during the spring months from 1990 to 1999 to linear jet streak quadrants aloft. They found that, in the entrance region of jet streaks, tornados occurred twice as often under the right entrance quadrant than under the left entrance quadrant. In the exit region, they found that tornados were much more likely to occur in the left exit region than in the right exit region. When considering all of the quadrants together, though, they found that tornados were twice as likely to form in the exit region as in the entrance region. During tornado "outbreaks" (cases where six or more tornados were associated with a storm system between 2100 to 0300 UTC), 73% more tornados occurred in the right exit region than in the right entrance region. This finding does not seem to agree with the linear jet streak theory, because the downward motion in the right exit region should decrease the likelihood of tornados, while the upward motion in the right entrance region should promote tornadogenesis.

Rose et al. (2003) also studied the density of tornado occurrences under jet streaks for this study period. When considering tornado reports from both outbreak and non-outbreak cases, there was a large maximum covering parts of both exit regions near the jet axis. A weaker maximum was seen in the right entrance quadrant. For the tornado outbreak cases, results were similar, but the maxima in the non-outbreak cases were more diffuse. Weak maxima were centered in the left exit region and right entrance region in the non-outbreak cases. By considering the tornado density's vicinity to the jet center, it was observed that tornados in the non-outbreak cases tended to be closer to the jet center than tornados from outbreak cases. When looking at outbreak cases alone, tornados in the entrance region usually were well upstream of the jet center, while tornados in the exit region were closer to the jet center than the entrance region tornados.

Using a method similar to Rose et al., Johnson-O'Mara (2006) found that, in the months from March to September over 10 years (1994 to 2003), tornado and hail reports most often occurred under the exit regions of jet streaks. He also observed that wind reports were more likely to occur under the right entrance and right exit quadrants, especially the right entrance quadrant.

Using the jet streak cases analyzed by Johnson-O'Mara, this study aims to further examine relationships between the jet streaks and storm reports. Specifically, it is expected that the tornado report density image created from this data will be consistent with the findings of Rose et al. (2003). It is also predicted that the jet quadrants with the highest average 250 mb divergence associated with storm reports will also have the largest number of storm reports. Finally, the average 250 mb divergence field is expected to agree with the linear jet streak theory.

3. Method

Data for this study were collected from the NCEP/NCAR NARR Reanalysis (Mesinger et al. 2006), SPC storm reports (NOAA 2007), and an analysis of linear jets by Johnson-O'Mara (2006). The storm reports used in this study occurred within a six-hour time period from 21 UTC to 3 UTC during the months from March until September of each year. Data gathered by the GrADS script used during the analysis included the month in which the jet was present, the latitude and longitude of each endpoint of the jet axes, and the number of tornado, hail, and wind reports in each jet quadrant. Data associated with storm reports included divergence at the location of the report and the quadrant in which the report was located. After a manual analysis of the data, a combination of FORTRAN programs and GrADS scripts was used to analyze the data and create related images. All results and images are in terms of a normalized jet streak which represents the findings from all cases considered.

By excluding the 412 cases without storm reports, the remaining 1112 cases were used to create storm report density images relative to the normalized jet streak. Seasonal images were created by dividing the reports according to month, and density images were also created for reports occurring before and after 00 UTC. By considering the angle of the jet axes, report density images were created for jets arriving from specific directions. In order to gain insight as to why the storm reports were distributed as they were and how circulations varied within the normalized area, average divergence images were created. In order to consider the effects of convection on jet streak circulations, an average divergence image was created for cases where storm reports were not present, and these results were compared to the average divergence field for cases with storm reports.

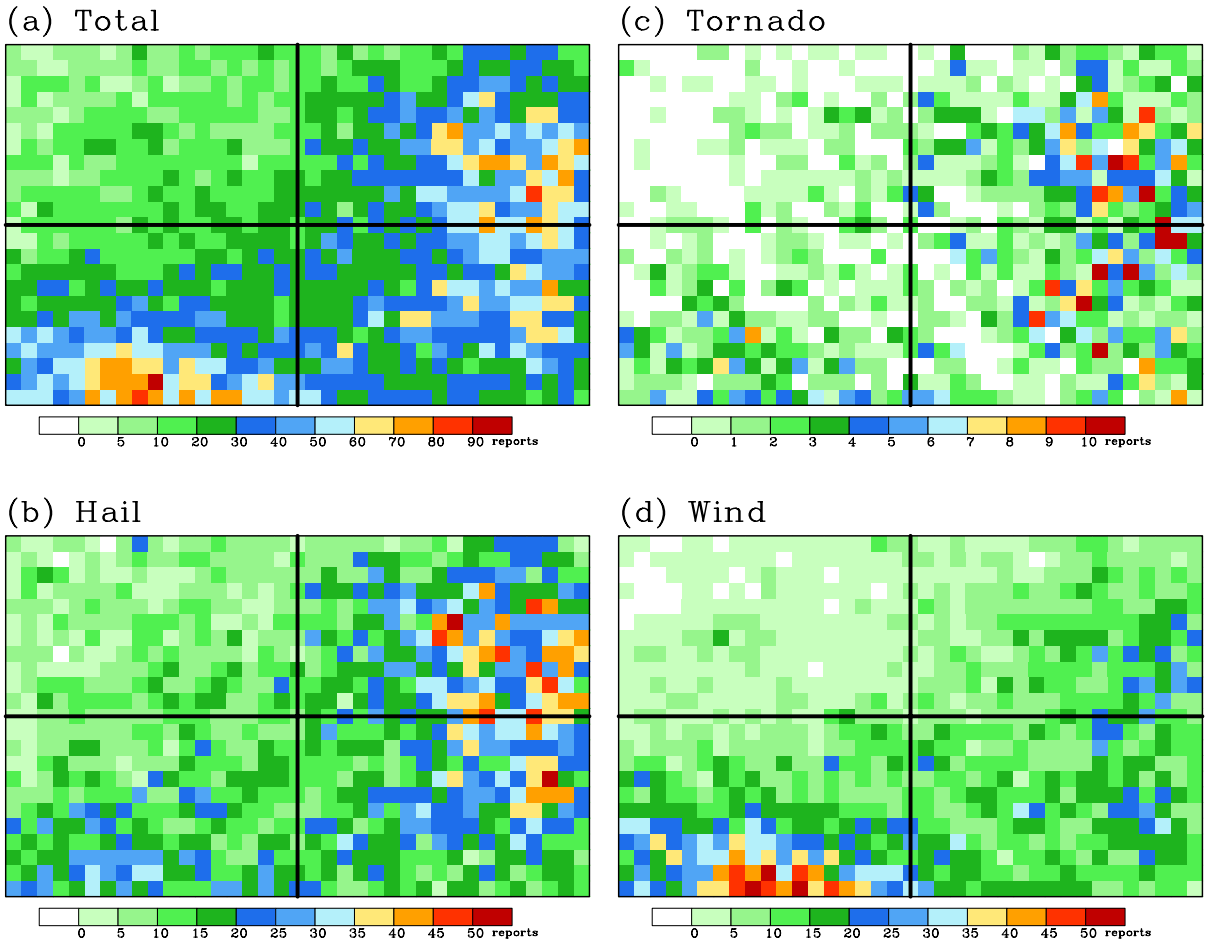

Fig. 2. Density plots for a) all reports, b) hail reports, c) tornado reports, and d) wind reports. The black lines in each image denote the jet axes, with the entrance region to the left and exit region to the right in each image. The quadrants have no set dimensions, because they represent a normalized area.

Mean sea level pressure was examined to observe how mean trends in boundaries and other features could affect the jet circulations and storm placement. Finally, wind vectors were plotted to observe how the circulations agreed with or differed from the linear jet streak theory.

4. Results

a. Overall storm densities

Fig. 2 shows storm report density within the normalized jet streak. When considering the placement of all storm reports within the normalized jet, two large maxima can be seen (Fig. 2a): one maximum is located far from the jet center through the left and right exit regions, while the other maximum is positioned far to the right in the right entrance region. By looking at the density plots for hail, tornados, and wind (Fig. 2b, 2c, and 2d, respectively), it is apparent that the hail and tornado reports are contributing to the exit region maximum, while the wind reports are primarily causing the right entrance region maximum. As shown in Table 1 (on the final page of the paper), the right entrance region of the normalized jet streak contained the most wind reports by far, and the left and right exit regions contain the bulk of the hail and tornado reports. The distribution of reports in Fig. 2c, the tornado report density image, is consistent with the findings of Rose et al. (2003). A strong maximum exists across the exit regions, while a weaker maximum is located in the right entrance region.

Table 1 shows the average 250 mb divergence associated with storm reports in each quadrant, in addition to the total number of

storm reports within each quadrant. It was expected that quadrants with larger average divergence aloft would also have a greater occurrence of storm reports because the associated upward motion would promote severe weather formation. When the 250 mb divergence is compared to the number of storm reports in each quadrant, we see that quadrants with the most storm reports are not necessarily the quadrants with the largest upper-level divergence. Table 1a shows that, overall, the region with that largest number of storm reports (the right exit region) is associated with the least amount of 250 mb divergence relative to other quadrants. The region with the least number of storm reports (by far) was the left entrance region, and this region had the second largest average divergence value. Table 1b, 1c, and 1d show that the strength of average divergence relative to the other quadrants is consistent through all four scenarios, though the proportions of storm reports change. The wind report scenario (Table 1d) is the only example where the largest divergence is also associated with the quadrant with the greatest amount of storm reports.

Confidence intervals were determined from the overall storm report data (Table 1a) in order to test whether the average divergence in each quadrant was significantly different to allow for meaningful comparisons. All confidence intervals provided evidence to reject the null hypothesis that the average divergence values between any two quadrants were equal, so the values differed enough to allow for comparison.

b. Seasonal storm densities

In order to observe when the tornado, hail, and wind reports were most likely to occur seasonally, the seven-month period was divided up into two seasons; Spring (March through May, shown in Fig. 3) and Summer (June through September, shown in Fig. 4). Statistically, 53% of all reports occurred in the Spring, while 47% occurred in the Summer.

The density images show that the exit region maximum is stronger in the Spring, and the right entrance region maximum is more apparent in the Summer. The reason why the exit region maximum is stronger in the Spring than in the Summer is because 60% of the tornado and hail reports occurred in the Spring, with the other 40% occurring during the Summer. The right entrance region maximum was stronger in the Summer than in the Spring because 43% of wind reports occurred in the Spring, while 57% occurred in the Summer. We would expect more tornadoes and reports of hail during the Spring, because the strong wind shear would promote tornado formation and the cold temperatures aloft would favor hail formation. Wind reports, however, should be more evenly distributed between Spring and Summer. This study has defined Spring to be a three-month period and Summer to be a four-month period, so each season would contain closer to 50% of the wind reports if each season were to be redefined as 3.5 months instead. Also, the Spring months would contain an even greater proportion of the tornado and hail reports if the months were categorized in this way. The wind report distribution may have been more meaningful if each of the months was examined individually.

c. Storm density by direction

In order to better understand how orientations of jet streaks affect the occurrence of severe weather, storm report densities were plotted for six directions (Fig. 5). Each of these six directions was defined to a 30 degree interval from 180 degrees (south) through 0 degrees (north). In other words, these six intervals contained every jet with a westward component. They also contained every possible direction that a jet streak could approach from in this study, because no jets in this study approached from the east. Fig. 5a shows that a jet approaching from the S to SSW direction would have the greatest potential for associated severe weather. This approach would be associated with a jet that is exiting a trough and in an area of positive vorticity advection (PVA).

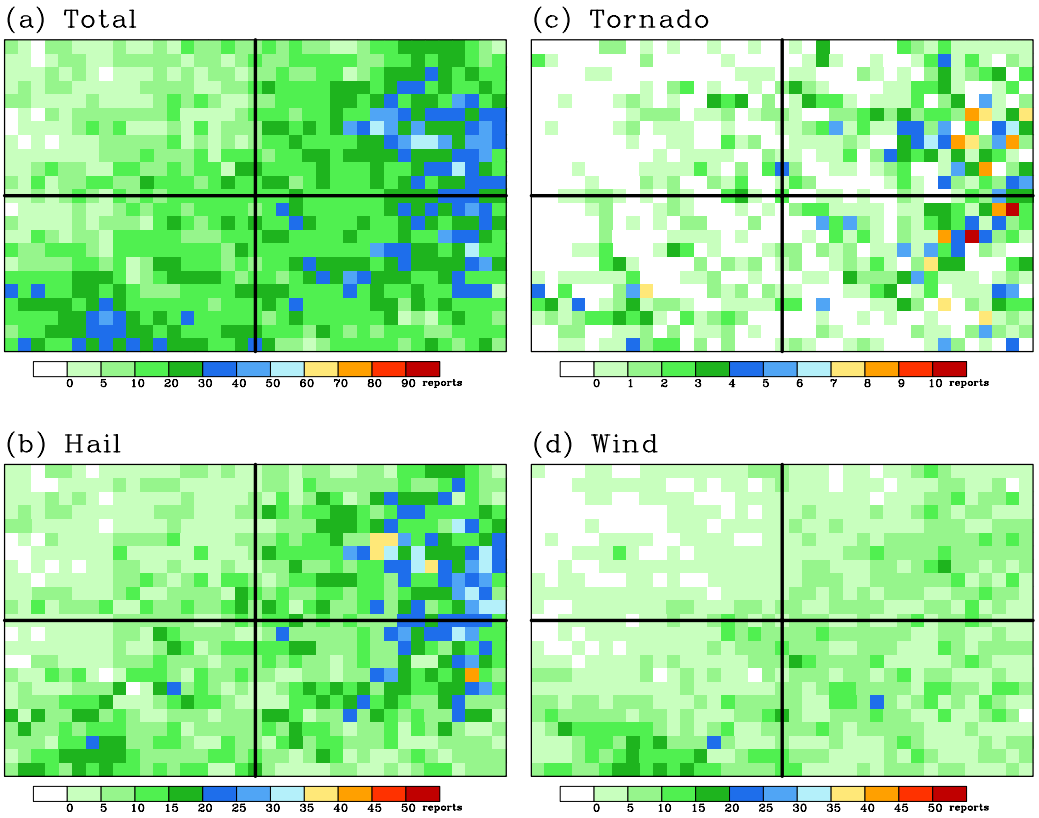

Fig. 3. Density plots for a) all reports, b) hail reports, c) tornado reports, and d) wind reports occurring during the Spring months (March, April, and May).

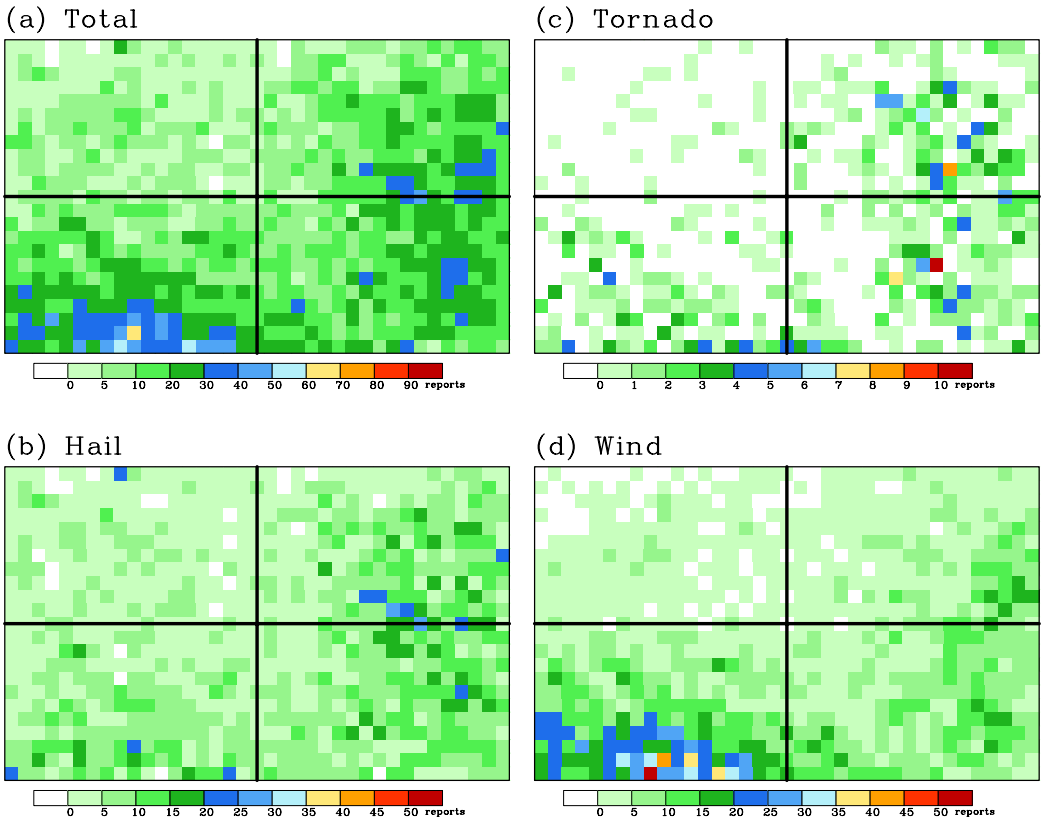

Fig. 4. Density plots for a) all reports, b) hail reports, c) tornado reports, and d) wind reports occurring during the Summer months (June, July, August, and September).

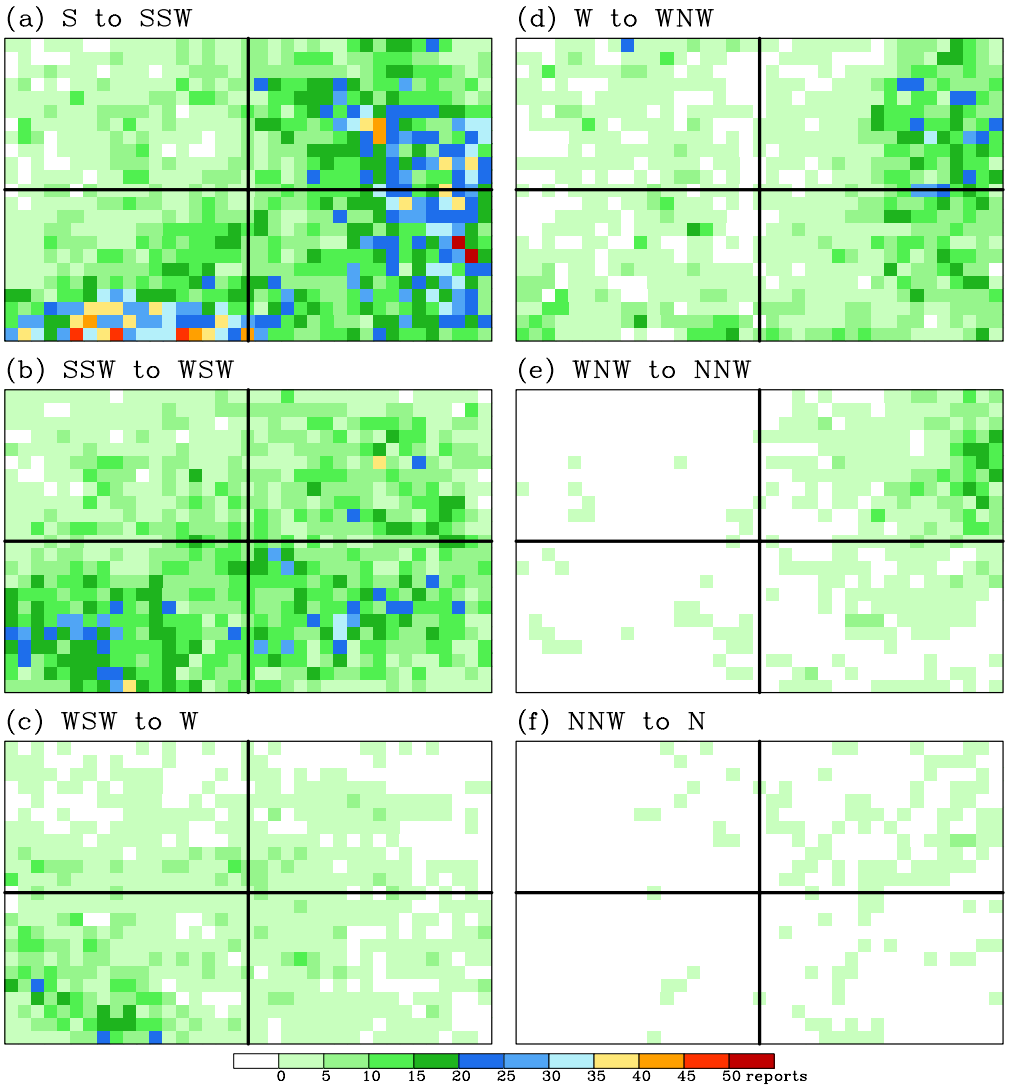

Fig. 5. Total storm report densities by direction.

This PVA, combined with the upward jet circulations, would promote the severe weather observed in the image. From earlier results regarding the distribution of storm reports in each maximum, it can be inferred that this type of jet is associated with a variety of severe weather, because both the exit maximum (associated with tornado and hail reports) and the right entrance maximum (associated with wind reports) are strong in Fig. 5a. The tornado/hail maximum is nearly centered between the two exit regions, while the wind maximum exists far from the major axis in the right entrance region.

The wind maximum has become more diffuse in the SSW to WSW image (Fig. 5b), and the tornado/hail maxima appear to be strongest in the right exit region. In the WSW to W image (Fig. 5c), the tornado/hail maximum has disappeared, but the wind maximum, though much weaker compared to the maximum in Fig. 5b, still exists. A strong maximum has re-established in the W to WNW image in the exit regions (Fig. 5d), though this maximum is positioned more in the left exit region than the right. The maximum remains, though weaker, for the WNW to NNW jet (Fig. 5e), and there is very little severe weather activity for jets coming from the NNW to N direction (Fig. 5f). Table 2 lists exactly how many storm reports were associated with each direction.

Fig. 6 shows density images from each of the directions for tornado reports alone. According to Table 2, most (41%) of the tornado reports were associated with jet streaks from the S to SSW direction. Fig. 6a shows that these

reports form a maximum in the exit regions as expected. This maximum is present again for jets from the W to WNW direction (Fig. 6d). Jet streaks from the SSW to WSW (Fig. 6b), however, contained twice as many storm reports as the jet streaks from the W to WNW directions, but showed very little preference for any quadrant. Even the left entrance quadrant, which typically has very few storm reports, appears to have more reports than usual in Fig. 6b when compared to the left entrance quadrants of jet streaks from other directions.

d. Storm densities before and after 00 UTC

In order to examine how many cases involved convection before 00 UTC, the cases were divided into before and after 00 UTC categories (recall that all storm reports in this study occurred within the 3 hours before and after 00 UTC). The results (seen in Fig. 7 and 8) showed that 56% of all reports occurred before 00 UTC and 44% occurred after 00 UTC.

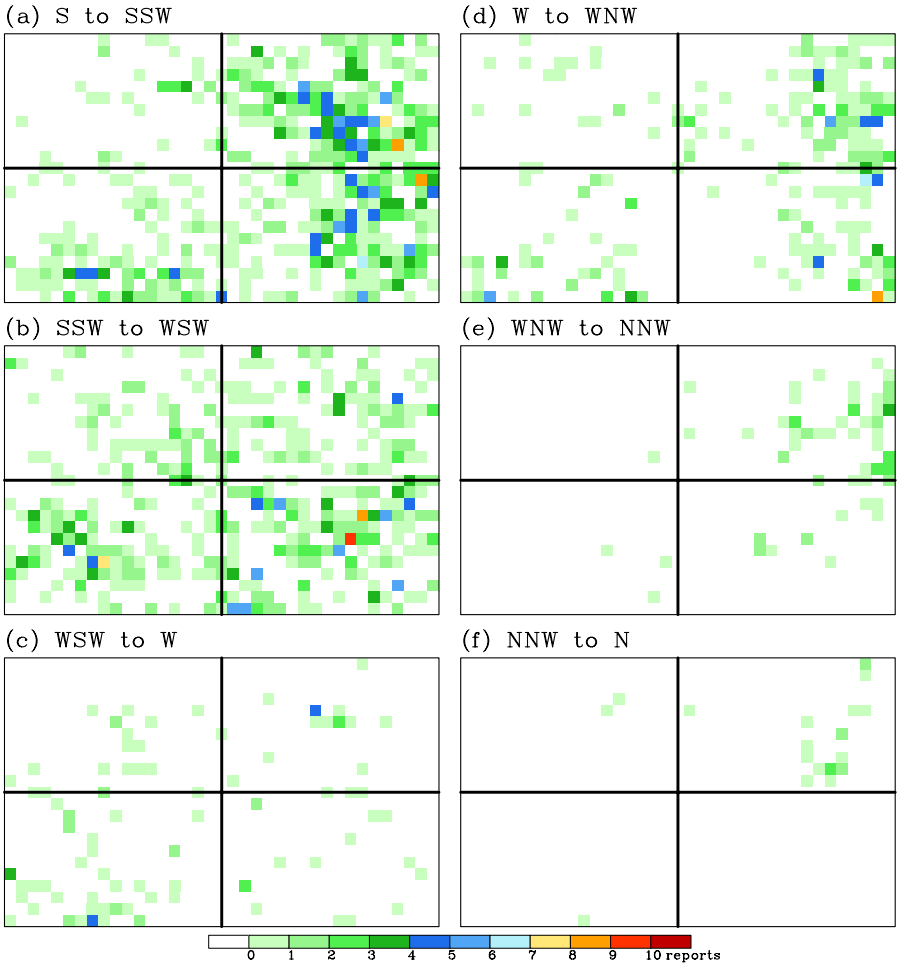

Fig. 6. Tornado report densities by direction.

Table 2. Number and percentage of storm reports from each direction.

	All	Tornado	Hail	Wind
S-SSW	11332 (41%)	831 (41%)	6167 (42%)	4334 (40%)
SSW-WSW	8001 (29%)	646 (32%)	4396 (30%)	2959 (28%)
WSW-W	2471 (9%)	115 (6%)	966 (7%)	1390 (13%)
W-WNW	4369 (16%)	323 (16%)	2491 (17%)	1555 (14%)
WNW-NNW	1197 (4%)	76 (4%)	724 (5%)	397 (4%)
NNW-N	234 (1%)	23 (1%)	109 (1%)	102 (1%)

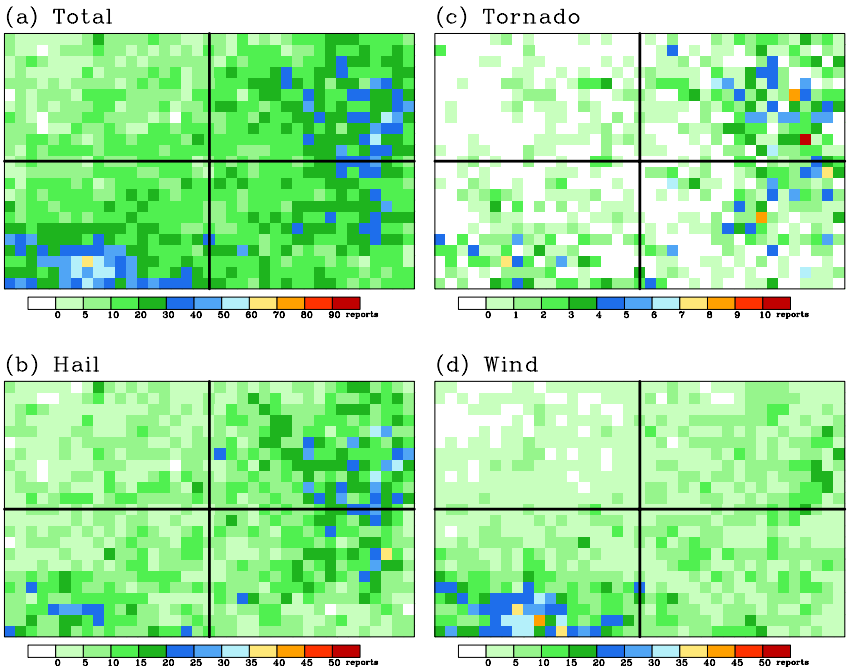

Fig. 7. Density plots for storm reports occurring before 00 UTC.

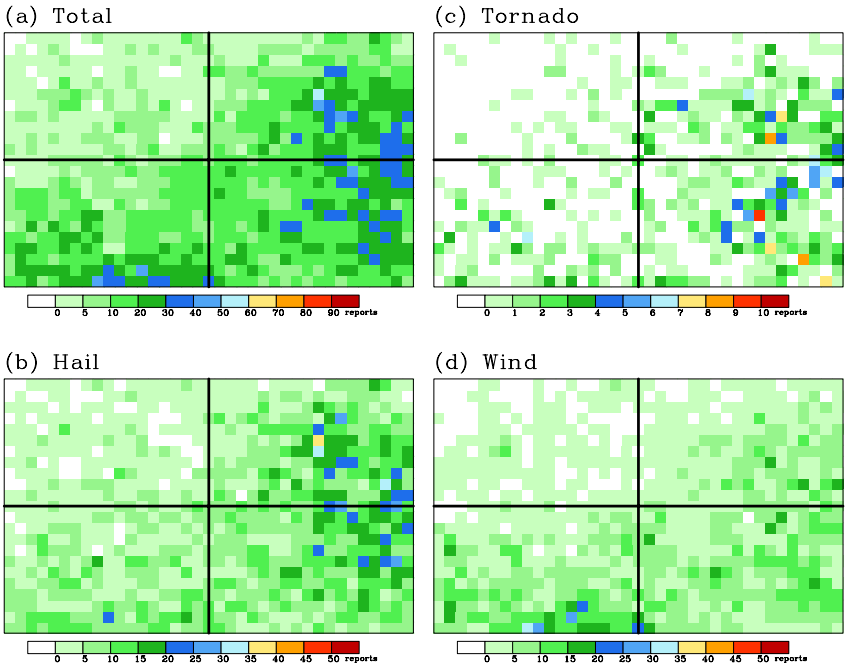

Fig. 8. Density plots for storm reports occurring after 00 UTC.

The percentages of tornado, hail, and wind report before and after 00 UTC were nearly identical to the percentages found overall. These percentages were exactly the same for hail and wind reports, while tornado reports showed very little difference with 57% before and 43% after 00 UTC. While the numbers before and after weren't remarkably different, the fact that the majority of the reports occurred before 00 UTC is significant, because the influence of convection from these storms may affect the observed divergence in the normalized area.

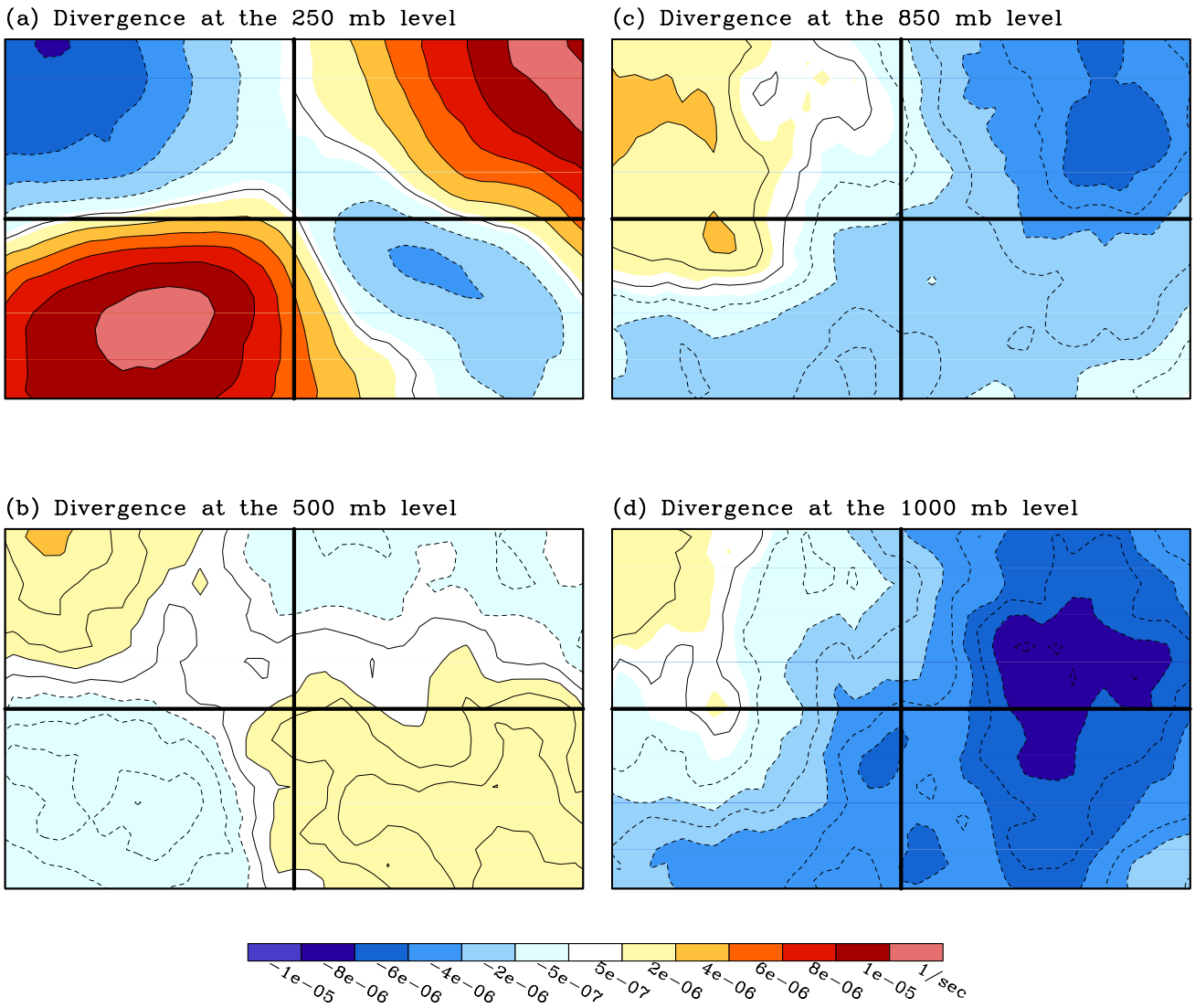

Fig. 9. Normalized average divergence at a) 250 mb, b) 500 mb, c) 850 mb, and d) 1000 mb, for cases with storm reports. The dashed lines denote areas of negative divergence (convergence).

e. Divergence in the normalized jet streak

1) PRESSURE LEVEL OBSERVATIONS

Fig. 9 shows the average divergence present at multiple pressure levels in the normalized area at 00 UTC for cases with storm reports. At the 250 mb level (Fig. 9a), there is divergence in the right entrance and left exit regions, and convergence in the left entrance and right exit regions. This verifies the linear jet streak theory explained and proven by researchers in the past (Sechrist and Whittaker 1979; Uccellini and Johnson 1979; Bluestein and Thomas 1984; Keyser and Johnson 1984; Hakim and Uccellini 1992; Moore and Vanknowe 1992). In this ten-year average, we see that the divergence maximum in the right entrance region is centered within the quadrant, while the divergence maximum in the left exit quadrant is in the farthest corner of the quadrant from the jet center. Though the convergence maxima are weaker than the divergence maxima, the positioning of maxima are similar; the convergence maximum in the right exit quadrant is located towards the center of the quadrant, while the convergence maximum in the left entrance quadrant is located in the quadrant's farthest corner away from the jet center.

At the 500 mb level (Fig. 9b), the divergence and convergence have weakened considerably compared to the values at the 250

mb level due to the 500 mb level's proximity to the level of nondivergence (Boyle and Bosart 1986). The level of nondivergence occurs where convergence and divergence cease, so it is understandable why convergence and divergence are so weak in this image. The areas of convergence and divergence at 500 mb are also opposite what they were at 250 mb. Despite this change, the positioning described at 250 mb can still be seen at 500 mb. As we examine levels closer to the surface (Fig. 9c and 9d), we see that an area of convergence exists in the exit regions, while an area of divergence can be seen in the left entrance region. According to the linear jet streak theory, there should be divergence at the surface in the right exit region, not convergence (as seen in this image). This disagreement is very likely associated with the fact that so many storm reports occurred in the right exit region. Convergence at the surface leads to upward motion, and upward motion promotes storm formation, so this surface convergence would promote storm formation in an area where storm development is suppressed by jet dynamics. The large surface convergence could also be evidence of a low pressure center, and the weaker low-level divergence could represent high pressure at the surface; this assumption will be examined later when the average mean sea level pressure is examined.

Spatial correlations were computed from the storm report data shown in Fig. 2 and the overall divergence data shown in Fig. 9. The spatial correlation between the number of storm reports and the 250 mb level divergence was 0.42, and the correlation between storm reports and the 850 mb level divergence was -0.59. At the 250 mb level, positive divergence values would be associated with storm reports, so it is understandable that a positive correlation was found. Likewise, the 850 mb level would have negative divergence (convergence) associated with storm reports, so the negative correlation was also expected. It is unclear, though, why the 850 mb negative correlation is stronger than the 250 mb positive correlation.

2) CROSS SECTION OBSERVATIONS

By looking at cross sections of the divergence field, trends between the pressure levels can be seen. The top image in Fig. 10 shows where the cross sections were taken within the normalized jet streak. In Latitudinal Cross Section 1 (Fig. 10a), we see the divergence dipoles in both the left entrance and left exit quadrants. We can also see that the areas of divergence and convergence are separated near the 400 mb level. In Latitudinal Cross Section 2 (Fig. 10b), there are two dipoles in the right exit region. The 400 mb level in this quadrant separates the dipoles; the dipole above 400 mb appears to have approximately equivalent areas and magnitudes of divergence and convergence, while the dipole below 400 mb has its convergence restricted to the lowest levels. Longitudinal Cross Section 1 (Fig. 10c) and Longitudinal Cross Section 2 (Fig. 10d) show the divergence of the entrance and exit regions, respectively. It should also be noted that Fig. 10d shows how the height of the tropopause changes with latitude. Air moving upward typically cannot continue to rise through the stable air of the tropopause, so the air must diverge; Fig. 10d shows that the areas of divergence associated with the tropopause exist at higher altitudes in the warm southern latitudes (on the left side of the image).

3) CONVECTION OBSERVATIONS

Recall that 56% of storm reports over the ten year period occurred before 00 UTC. The divergence images were from 00 UTC, so, at the very least, the convection from 56% of the storm reports had the opportunity to affect the divergence field. In order to gauge how that convection modifies the divergence, a separate

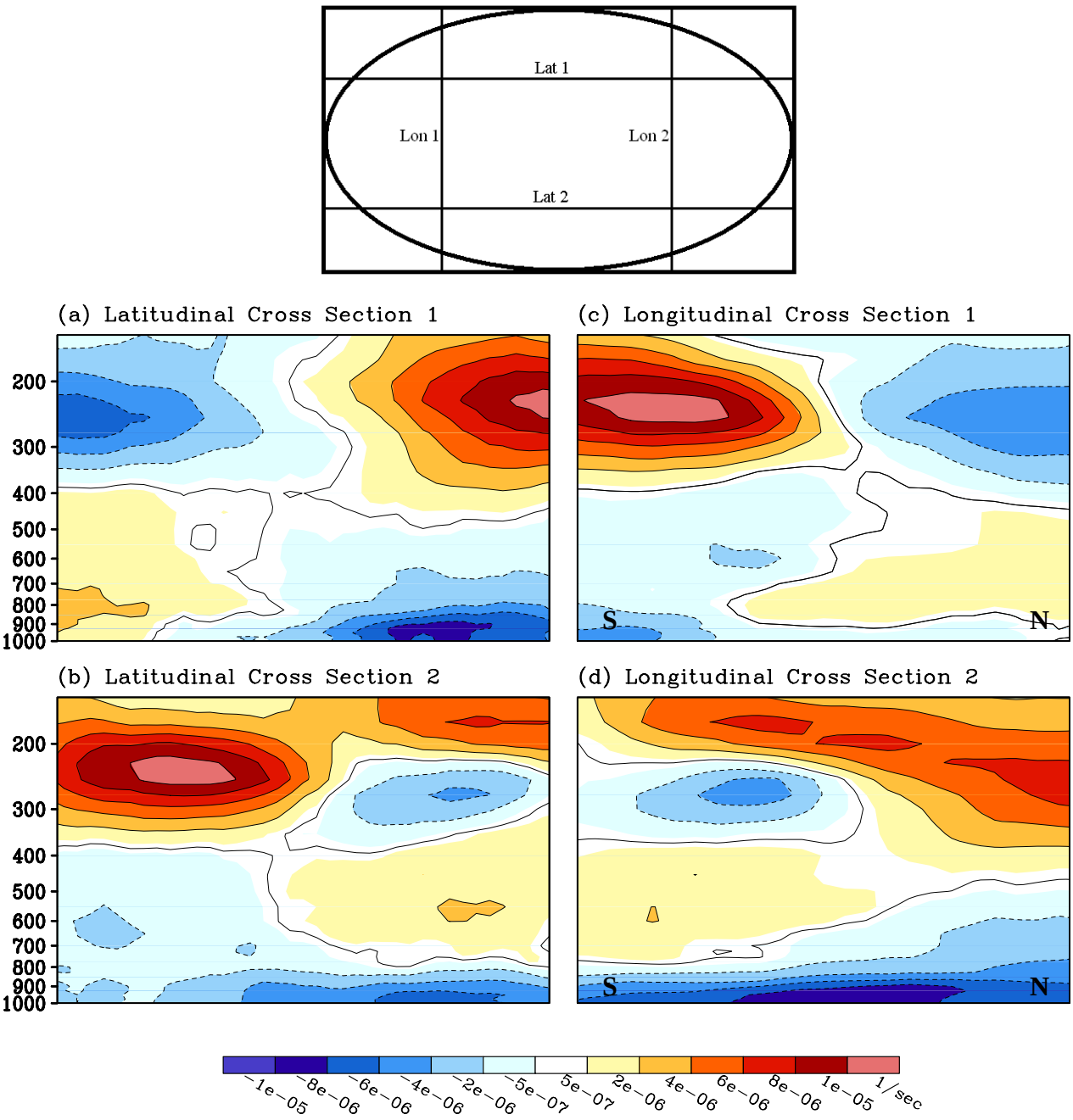

Fig. 10. Cross sections from the normalized average divergence field for cases with storm reports, with cross section slides as described in the top image. The mb levels are shown to the left of the cross sections.

divergence field was observed from 412 jet streak cases where there were no associated storm reports. This divergence field (Fig. 11) shows similarities to Fig. 9.

Both the 250 mb and 500 mb images show the same general divergence/convergence pattern as the images with storm reports. The "report-less" 250 mb image (Fig. 11a) shows convergence and divergence maxima of similar magnitudes, while the image including reports (Fig. 9a) shows the divergence maxima to be larger in magnitude than the convergence maxima. The "report-less" image shows that the divergence in the right entrance and left exit regions is weaker than in the image with storm reports, while the convergence in the left entrance and right exit regions of the "report-less" image is stronger than in the image with storm reports. It appears, then, that the storm convection has a slight affect on the divergence field, amplifying divergence while suppressing convergence aloft.

In Fig. 11b, the level of nondivergence (Boyle and Bosart 1986) can again be seen near the 500 mb level. Closer to the surface in the "report-less" image (Fig. 11c and 11d), there is much less convergence at the surface than there was in the surface images with storm reports (Fig. 9c and 9d). This implies that the surface convergence seen in Fig. 9 was associated with the storm reports, because this surface convergence is not nearly as strong in the images without storm reports.

f. Average mean sea level pressure

In order to better understand the previous images, an average mean sea level pressure image was created (Fig. 12) from the cases with storm reports. This figure shows that a low pressure center exists in the left exit region of the normalized jet streak. The jet circulations provide upward motion in the left exit region, which lowers the pressure in this quadrant, making it suitable for the development of a low pressure center. The low's presence confirms what was seen in Fig. 9d, where there was a large area of surface convergence associated with the low in the left exit region.

The average position of a front can be inferred in Fig. 12. Following the enhanced troughing in the isobars, it can be seen that the front is most likely to extend from the left exit region into the right exit and right entrance regions. The position of the front explains the placement of the maxima in Fig. 2; storm reports are likely occurring in the proximity of the front, so maxima exist in the exit regions and the right entrance region. The left entrance region has the fewest storm reports by far, and this makes sense when we notice that the front would likely be farthest from this region.

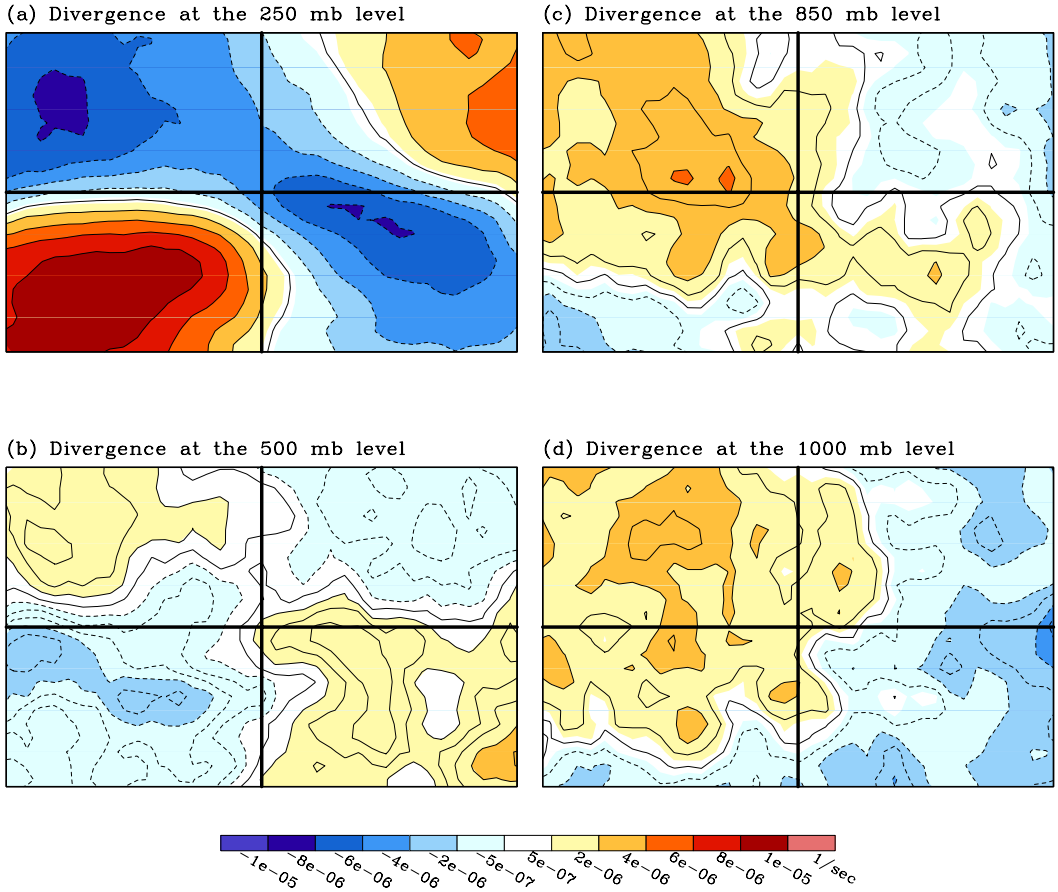

Fig. 11. Normalized average divergence for cases without storm reports.

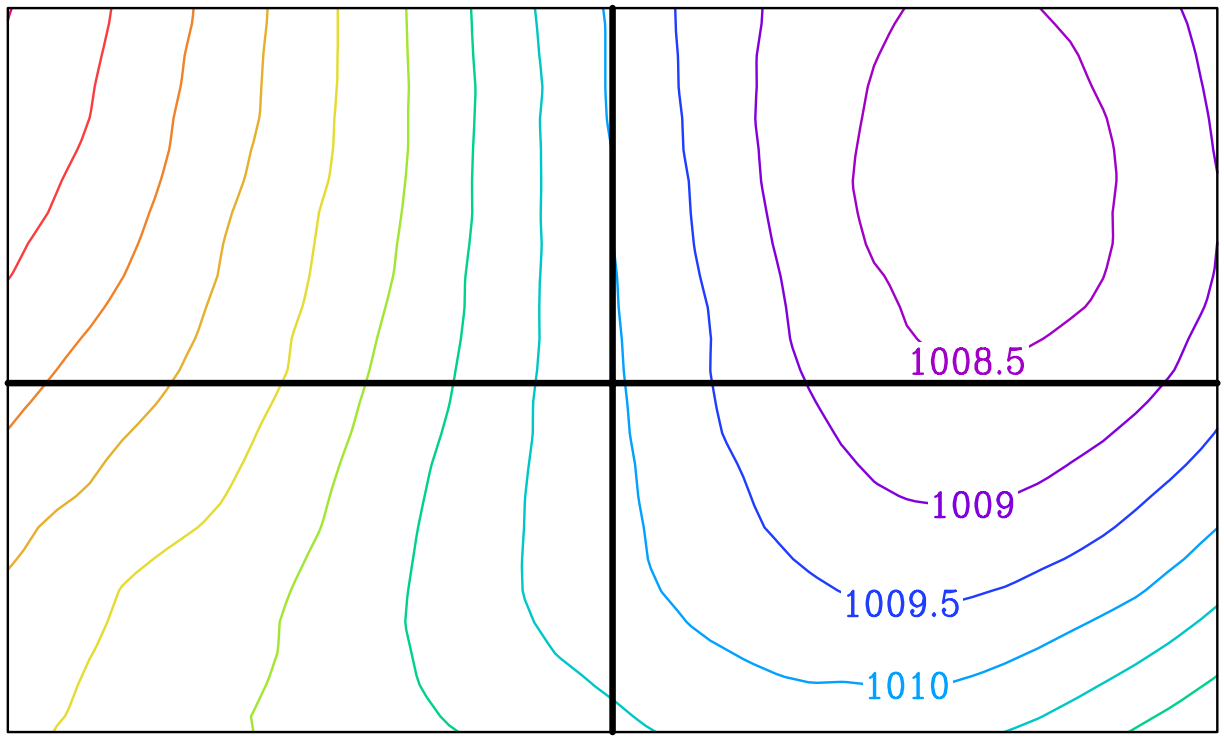

Fig. 12. Normalized mean sea level pressure in mb.

Finally, the image hints at the presence of a high pressure center northwest of the normalized left entrance region. High pressure suppresses upward motion, so this may be another reason why there were so few storm reports in the left entrance quadrant.

g. Wind vectors

1) HORIZONTAL WINDS

Fig. 13 shows the horizontal wind vectors in the normalized jet streak at various pressure surfaces, with the magnitude of the vectors shaded in the background. The 250 mb surface (Fig. 13a) shows the typical jet streak shape, with a wind maximum at the center of the image and decreasing wind speeds away from the axis center. This verifies that Johnson O'Mara was accurate in analyzing the jet streaks. This image also shows that there is a west-southwest wind across the 250 mb surface. It is unknown exactly why the winds throughout the layer would move in the west-southwest direction; the wind does not appear to be specifically targeting the left exit region, and it would not be expected to because of the upper-level divergence in this quadrant. It may be possible that the image is simply reflecting the tendency for jets to have a west-southwest component of the horizontal wind.

Fig. 13b shows that the wind maximum at the 500 mb layer is displaced into the right entrance and exit quadrants, and the winds continue to move in the west-southwest direction. In the 850 mb image (Fig. 13c), the wind directions are quite varied, depending on their position within the normalized area. The winds do appear to be aimed to the left of the left exit region, presumably converging at the low, as wind magnitudes decrease as the winds approach this area. The 1000 mb image (Fig. 13d) shows a similar trend, but there is one noticeable difference between the 850 mb and 1000 mb images: the wind maximum in the 850 mb image is in the right exit region, while the left entrance region contains the maximum in the 1000 mb image. While these images are at a low enough level that we can expect convergence in the left exit region because of the low pressure system addressed earlier, the vectors still appear to be aimed past where the low was expected.

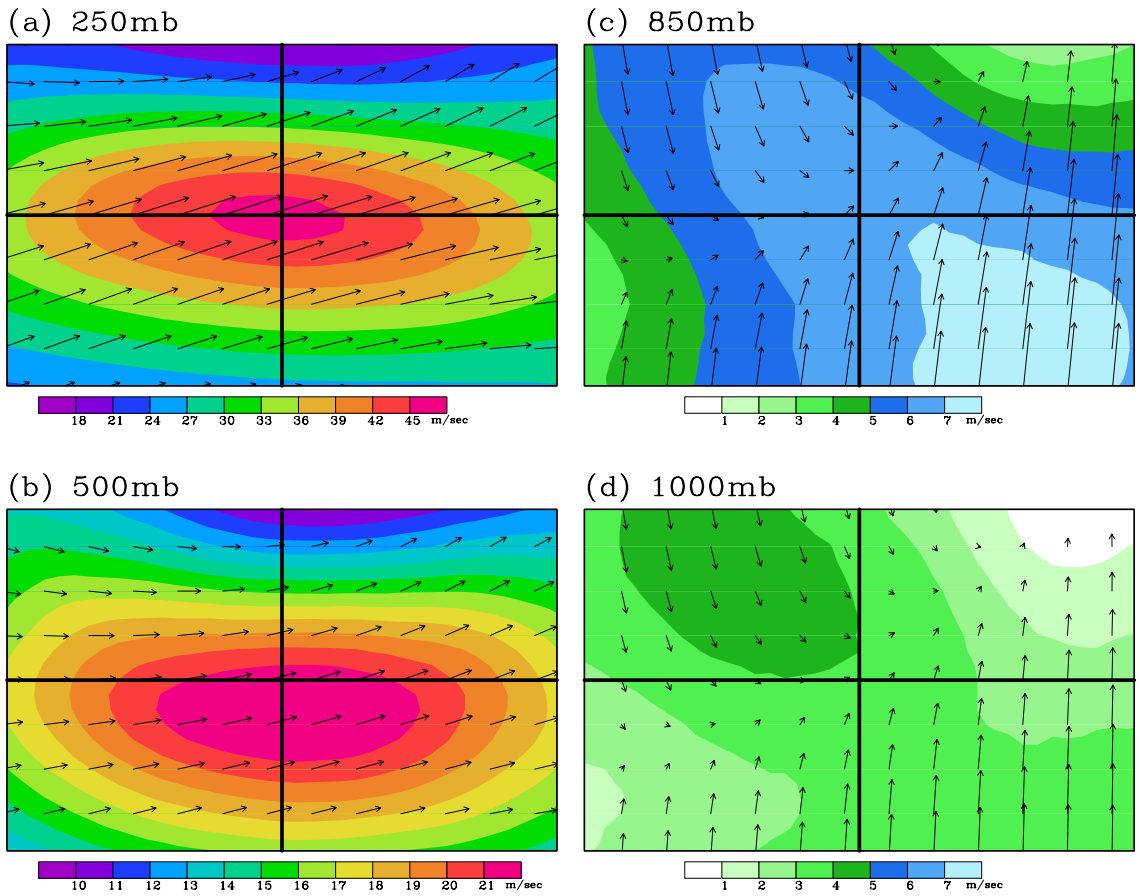

Fig. 13. Horizontal wind vectors at a) 250 mb, b) 500 mb, c) 850 mb, and d) 1000 mb, with the magnitude of the vectors shaded in the background.

2) VERTICAL WINDS

Fig. 14 and Fig. 15 show cross sections depicting vertical wind with the wind magnitude and divergence in the background, respectively. Latitudinal Cross Section 1 (Fig. 14a and 15a), taken again through the left entrance and left exit regions, shows that winds (in this image) are strongest aloft in the left entrance region, where there is convergence aloft. The u-component of the wind depicted in this latitudinal image is oriented towards the exit region as discussed previously. Winds below this maximum have a downward component, which is expected because of the convergence aloft and divergence near the surface (Fig. 15a).

Latitudinal Cross Section 2 (Fig. 14b and 15b), through the right entrance and right exit regions, shows the wind maximum (not surprisingly) aloft, with a horizontal component again directed eastward. The most important feature of this image is that there is rising motion everywhere. From the divergence field and the sheer number of storm reports in the right exit region, it was inferred that there would be an upward motion in this quadrant, and this upward motion is confirmed in this image. The average convergence aloft isn't strong enough to force a downward motion. The mean sea level pressure image showed that a front would be present in this region, so it is likely that the upward motion associated with the front is influencing the circulation.

Longitudinal Cross Section 1, taken through the entrance regions, shows the classic direct circulation described by researchers previously (Fig. 14c and 15c). Air ascends in the right entrance region, moves into the left entrance region aloft, then descends in this region. Once the air reaches the surface again, it moves

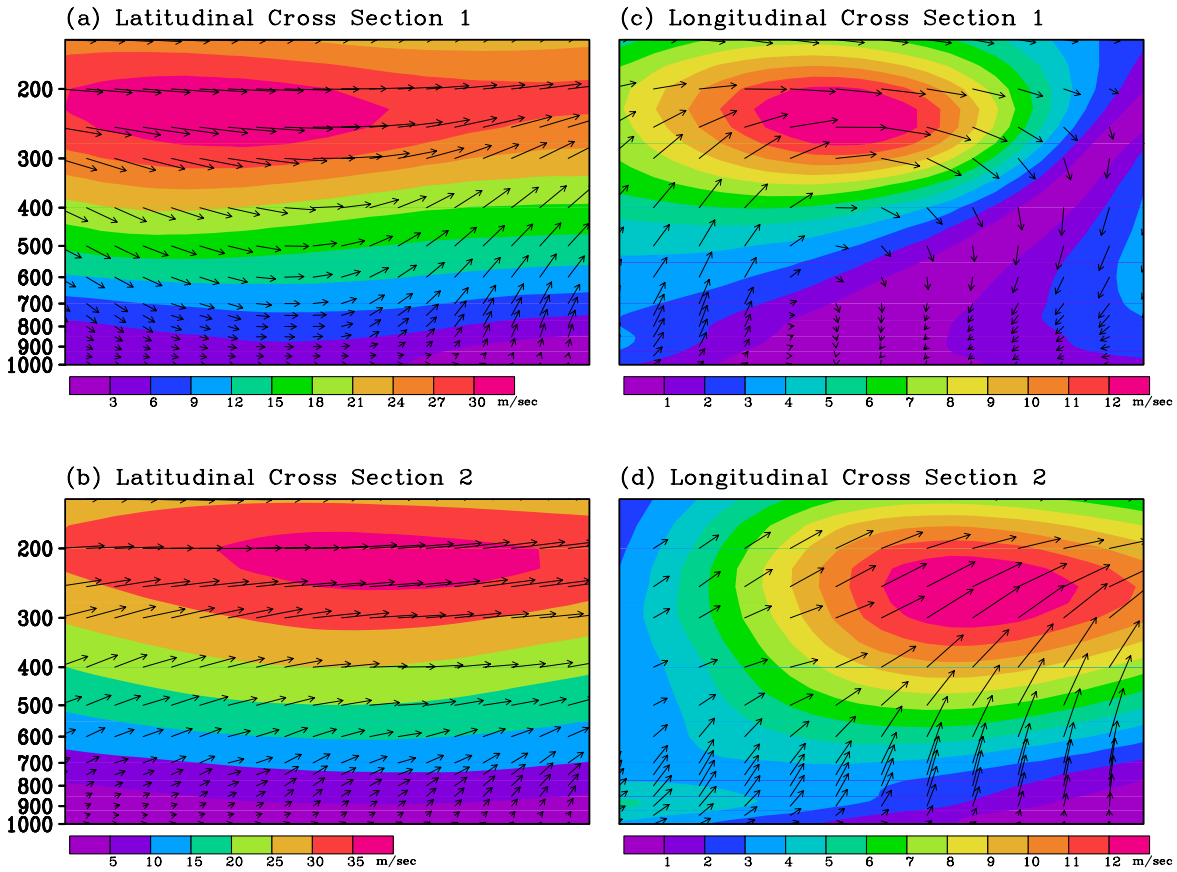

Fig. 14. Vertical wind vector cross sections with shaded wind magnitudes. Cross sections taken as shown in Fig. 11.

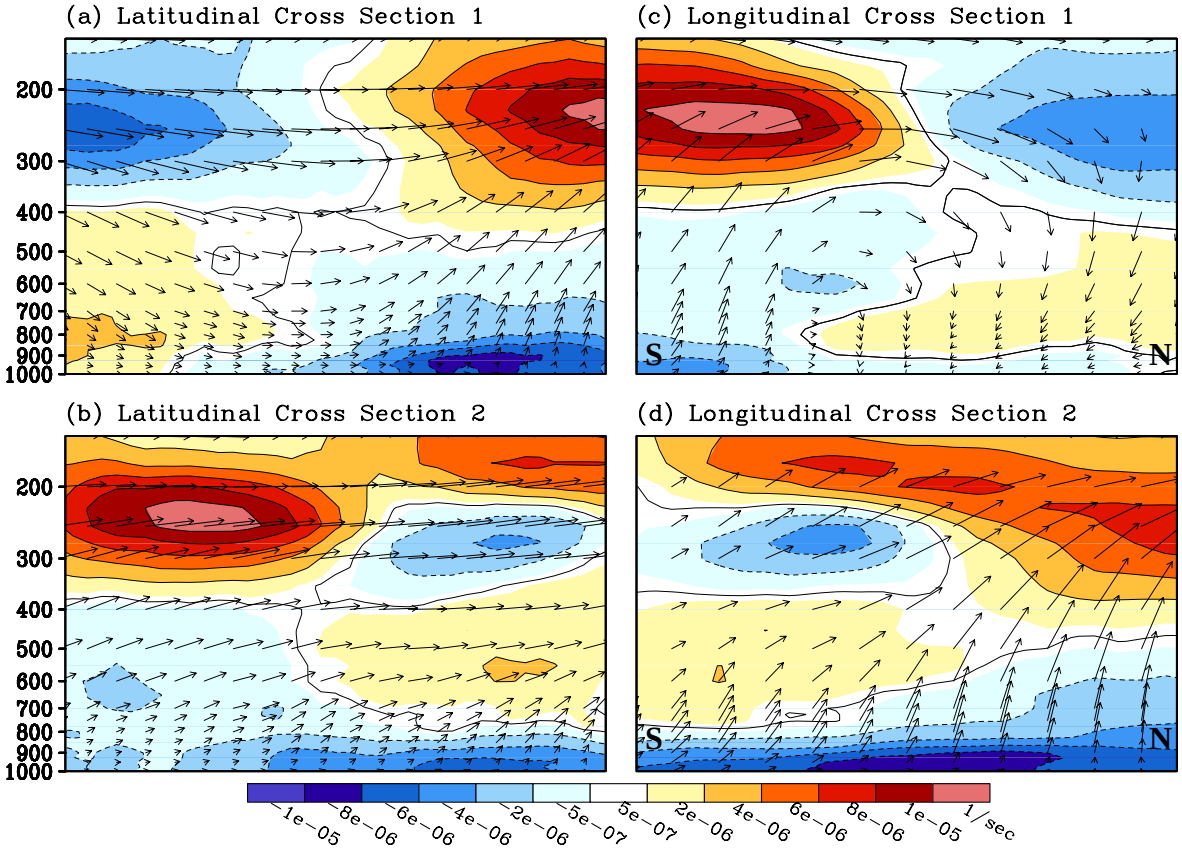

Fig 15. Vertical wind vector cross sections with shaded divergence. Cross sections taken as shown in Fig. 11.

weakly toward the right entrance region again. Fig 15c shows that this weak movement of air dominates the area near the surface where the quadrants meet.

Longitudinal Cross Section 2 (Fig. 14d and 15d), taken through the exit regions, is similar to Latitudinal Cross Section 2 in that it also does not show any downward motion. The only quadrant with a downward wind component was the left entrance region, and the right exit region has upward motion despite the expected downward motion from the jet streak. Fig. 15d shows that the upward component of the wind is stronger in the left exit region, as it should be (according to the linear jet streak theory). The small area of convergence in the right exit region does affect the vertical motion, but it doesn't have a large enough effect to induce downward motion.

5. Conclusion

The ten-year normalized jet streak images provide insight into the storm distributions and atmospheric circulations associated with linear jet streaks. From density images, it was seen that tornado and hail reports formed a maximum in the exit regions far from the jet center, while a wind report maximum occurred in the right entrance region far from the major axis. The tornado report density maximum in the exit region was consistent with the findings of Rose et al (2003). Quadrants with the largest average storm report divergence did not necessarily have the largest amount of storm reports, as was expected in this study. Both the exit maximum and right entrance maximum were stronger in the three hours before 00 UTC than after, and the exit region maximum was stronger during the Spring months than in the Summer months. A low pressure center in the left exit region was consistent with the extensive surface convergence, and fronts associated with the low appeared to be a major reason for the storm report distributions observed. Divergence at the 250 mb level agreed with linear jet streak theory, though circulations were influenced by pressure centers, fronts, the tropopause, and convection.

Future research should examine a larger normalized area. By doing so, it may be possible to view a high pressure center past the left entrance region and a warm front ahead of the low. It may also be informative to consider the surface temperature gradient in the normalized area to see if temperature gradients match the pressure gradients used to identify fronts in the present study. Ageostrophic wind vectors and vorticity could also be plotted to further investigate circulations associated with the jet streaks. Finally, studying the relationship between the divergence associated with storm reports and the number of storm reports in a quadrant could be beneficial, because the study showed that quadrants with higher divergence may not necessarily have a higher occurrence of storm reports.

Acknowledgments. I would like to thank Adam Clark for his guidance and programming expertise, and Dr. Gallus for his help regarding the direction of the research. I thank Dave Flory and Daryl Herzmann for their computational assistance and Kaj Johnson-O'Mara for his advice throughout the project.

6. References

Bluestein, H. B., and K. W. Thomas, 1984: Diagnosis of a jet streak in the vicinity of a severe weather outbreak in the Texas panhandle. *Mon. Wea. Rev.*, **112**, 2499-2520.

Boyle, J. S., and L. F. Bosart, 1986: Cyclone–Anticyclone Couplets over North America. Part II: Analysis of a Major Cyclone Event over the Eastern United States. *Mon. Wea. Rev.*, **114**, 2432–2465.

Brill, K. F., L. W. Uccellini, R. P. Burkhart, T. T. Warner, and R. A. Anthes, 1985: Numerical simulations of a transverse indirect circulation and low-level jet in the exit

region of an upper-level jet. *J. Atmos. Sci*., **42**, 1306-1320.

Hakim, G. J., and L. W. Uccellini, 1992: Diagnosing coupled jet-streak circulations for a northern plains snow band from the operational nested-grid model. *Wea. Forecasting*, **7**, 26-48.

Johnson-O'Mara, K., 2006: Diagnosis of severe storm reports in comparison to upper-level linear jet streak quadrants. Undergraduate thesis, Dept. of Geological and Atmospheric Sciences, Iowa State University, 7 pp.

Keyser, D. A., and D. R. Johnson, 1984: Effects of diabatic heating on the ageostrophic circulation of an upper tropospheric jet streak. *Mon. Wea. Rev.*, **112**, 1709-1724.

Mesinger, F., G. DiMego, E. Kalnay, K. Mitchell, P. C. Shafran, W. Ebisuzaki, D. Jović, J. Woollen, E. Rogers, E. H. Berbery, M. B. Ek, Y. Fan, R. Grumbine, W. Higgins, H. Li, Y. Lin, G. Manikin, D. Parrish, and W. Shi, 2006: North American Regional Reanalysis. *Bull. Amer. Meteor. Soc.*, **87**, 343–360.

Moore, J. T., and G. E. Vanknowe, 1992: The effect of jet-streak curvature on kinematic fields. *Mon. Wea. Rev*., **120**, 2429-2441.

NOAA, cited 2007: Climatological or Past Storm Information. [Available online at http://www.spc.noaa.gov/climo/historical.html/.]

Rose, S. F., P. V. Hobbs, J. D. Locatelli, and M. T. Stoelinga, 2003: A 10-yr climatology relating the locations of reported tornadoes to the quadrants of upper-level jet streaks. *Wea. Forecasting*, **19**, 301-309.

Sechrist, F. S., and T. M. Whittaker, 1979: Evidence of jet streak vertical circulations. *Mon. Wea. Rev*., **107**, 1014-1021.

Uccellini, L. W., and D. R. Johnson, 1979: The coupling of upper and lower tropospheric jet streaks and implications for the development of severe convective storms. *Mon. Wea. Rev*., **107**, 682-703.

Uccellini, L. W., and P. J. Kocin, 1987: The interaction of jet streak circulations during heavy snow events along the east coast of the United States. *Wea. Forecasting*, **2**, 289-308.

Table 1. The number of a) total reports, b) tornado reports, c) hail reports, and d) wind reports, as well as the average associated divergence, in each quadrant.

a) All Reports

Left Entrance Quadrant Storm Reports: 2802 (4th most, 10.14%) Divergence: 1.80×10^{-5} sec^{-1} (2nd largest)	Left Exit Quadrant Storm Reports: 7983 (3rd most, 28.92%) Divergence: 1.52×10^{-5} sec^{-1} (3rd largest)
Right Entrance Quadrant Storm Reports: 8363 (2nd most, 30.30%) Divergence: 2.74×10^{-5} sec^{-1} (Largest)	Right Exit Quadrant Storm Reports: 8456 (Most, 30.63%) Divergence: 9.68×10^{-6} sec^{-1} (4th largest)

b) Tornado Reports

Left Entrance Quadrant Storm Reports: 176 (4th most, 8.74%) Divergence: 2.10×10^{-5} sec^{-1} (2nd largest)	Left Exit Quadrant Storm Reports: 709 (Most, 35.20%) Divergence: 1.57×10^{-5} sec^{-1} (3rd largest)
Right Entrance Quadrant Storm Reports: 445 (3rd most, 22.10%) Divergence: 2.95×10^{-5} sec^{-1} (Largest)	Right Exit Quadrant Storm Reports: 684 (2nd most, 33.96%) Divergence: 1.04×10^{-5} sec^{-1} (4th largest)

c) Hail Reports

Left Entrance Quadrant Storm Reports: 1873 (4th most, 12.61%) Divergence: 1.63×10^{-5} sec^{-1} (2nd largest)	Left Exit Quadrant Storm Reports: 4972 (Most, 33.47%) Divergence: 1.25×10^{-5} sec^{-1} (3rd largest)
Right Entrance Quadrant Storm Reports: 3466 (3rd most, 23.34%) Divergence: 2.44×10^{-5} sec^{-1} (Largest)	Right Exit Quadrant Storm Reports: 4542 (2nd most, 30.58%) Divergence: 7.86×10^{-6} sec^{-1} (4th largest)

d) Wind Reports

Left Entrance Quadrant Storm Reports: 753 (4th most, 7.01%) Divergence: 2.16×10^{-5} sec^{-1} (2nd largest)	Left Exit Quadrant Storm Reports: 2302 (3rd most, 21.44%) Divergence: 2.09×10^{-5} sec^{-1} (3rd largest)
Right Entrance Quadrant Storm Reports: 4452 (Most, 41.46%) Divergence: 2.94×10^{-5} sec^{-1} (Largest)	Right Exit Quadrant Storm Reports: 3230 (2nd most, 30.08%) Divergence: 1.21×10^{-5} sec^{-1} (4th largest)